

Hinge solitons in three-dimensional second-order topological insulators

Yu-Liang Tao¹, Ning Dai¹, Yan-Bin Yang¹, Qi-Bo Zeng¹, and Yong Xu^{1,2*}

¹*Center for Quantum Information, IIIS, Tsinghua University, Beijing 100084, People's Republic of China and*

²*Shanghai Qi Zhi Institute, Shanghai 200030, People's Republic of China*

Higher-order topological insulators have recently witnessed rapid progress in various fields ranging from condensed matter physics to electric circuits. A well-known higher-order state is the second-order topological insulator in three dimensions with gapless states localized on the hinges. A natural question in the context of nonlinearity is whether solitons can exist on the hinges in a second-order topological insulator. Here we theoretically demonstrate the existence of stable solitons localized on the hinges of a second-order topological insulator in three dimensions when nonlinearity is involved. By means of systematic numerical study, we find that the soliton has strong localization in real space and propagates along the hinge unidirectionally without changing its shape. We further construct an electric network to simulate the second-order topological insulator. When a nonlinear inductor is appropriately involved, we find that the system can support a bright soliton for the voltage distribution demonstrated by stable time evolution of a voltage pulse.

I. INTRODUCTION

Solitons, solitary waves travelling without changing their shapes, result from the balance between dispersion and nonlinearity. Solitons exist in various nonlinear systems, such as nonlinear optics [1–3], Bose-Einstein condensates (BECs) [4–8] and Fermi superfluids [9–14]. They usually stably exist in a one-dimensional system. Yet, it is a challenging problem to create solitons, especially for a bright soliton with a wave density bump, in higher-dimensional systems. The difficulty lies in the fact that the nonlinear Schrödinger equation for the ubiquitous cubic local nonlinearity leads to critical and supercritical wave collapse [15, 16] in two and three dimensions, respectively. To generate stable higher-dimensional bright solitons, one can consider nonlocal nonlinearity, such as the nonlinearity resulted from the dipole-dipole interactions in BECs [17, 18], and modified kinetic energy, such as involving the spin-orbit coupling [19, 20]. An alternative perspective is to engineer solitons at the boundaries with lower dimension in a higher-dimensional system. Since topological insulators support lower dimensional edge states, they provide an ideal platform to realize the boundary-localized solitons. Indeed, such solitons have been theoretically predicted in a two-dimensional topological insulator with one-dimensional edges [21–33]. Remarkably, the topological edge solitons have been experimentally observed very recently [34–36]. Interestingly, solitons have also been numerically found in Weyl semimetals [37].

Traditional topological insulators in n dimensions support edge states localized at $(n - 1)$ -dimensional boundaries, such as the Chern insulator. Recently, topological phases have been generalized to the higher-order case where gapless edge states are localized at $(n - m)$ -dimensional (with $m > 1$) boundaries [38–67]. Such insulators are coined higher-order topological insulators,

or specifically, m th-order topological insulators. For instance, in two dimensions (2D), there exists type-I [40] and type-II [62] quadrupole topological insulators that support zero-energy modes localized at the corners. In three dimensions (3D), there exists a second-order topological insulator hosting chiral modes localized on the hinges, when an appropriate term breaking the time-reversal symmetry is involved in a \mathbb{Z}_2 topological insulator [50]. In the context of nonlinearity, it is natural to ask whether the second-order topological system can support solitons localized on the hinges when nonlinearity is involved.

Several higher-order topological phases have been experimentally observed in several systems [47, 48, 52, 53]. One of them uses electric circuits [53] which have been demonstrated to be a powerful platform to simulate various topological phases in lattice models, such as the Su-Schrieffer-Heeger model [68], topological nodal semimetals [69, 70], topological amorphous metals [71], non-Hermitian Aubry-André-Harper models [72, 73], two-dimensional higher-order topological phases [53, 62, 67] and others [74–83]. However, whether the electric circuits can be used to realize the 3D second-order topological insulator has not been explored. In addition, an electric network becomes nonlinear when either nonlinear capacitors or inductors (such as the nonlinear transmission lines) are involved, leading to electric solitons in the form of voltage waves [84–86]. One may wonder whether the electric circuit can support hinge solitons in the 3D second-order topological insulator.

In this paper, we theoretically predict the existence of solitons in a 3D second-order topological insulator when nonlinearity is involved. Such solitons result from the balance between nonlinearity and dispersion of the hinge modes. For the higher-order topological insulator, there are two regimes: strong regime with chiral hinge modes and weak regime with hinge modes that are not chiral. We find that the solitons can exist in both of these two regimes. Yet, we show that the soliton in the strong regime is more stable than the one in the weak regime, which gradually slows down. Furthermore, we propose a

* yongxuphy@tsinghua.edu.cn

scheme to realize the second-order topological insulator in electric circuits with nonlinearity that can be realized by a voltage-controlled variable inductor. By simulating the dynamics of the circuit, we finally show that a bright soliton can stably exist in the system.

II. LINEAR MODEL HAMILTONIAN

We start by considering the model described by the following Hamiltonian in momentum space [50]

$$H_L(\mathbf{k}) = (M + J \sum_{\nu=x,y,z} \cos k_\nu) \tau_z \sigma_0 + \Delta_1 \sum_{\nu=x,y,z} \sin k_\nu \tau_x \sigma_\nu + \Delta_2 (\cos k_x - \cos k_y) \tau_y \sigma_0, \quad (1)$$

where σ_ν and τ_ν represent Pauli matrices acting on different degrees of freedom, σ_0 and τ_0 refer to 2×2 identity matrices. J , M , Δ_1 and Δ_2 are real parameters. When $\Delta_2 = 0$, the Hamiltonian describes the 3D \mathbb{Z}_2 topological insulator [87]. It respects both time-reversal symmetry, i.e., $\mathcal{T}H(\mathbf{k})\mathcal{T}^{-1} = H(-\mathbf{k})$ with $\mathcal{T} = i\sigma_y\kappa$ (κ denotes the complex conjugation operator), and the rotational symmetry, i.e., $C_4^z H(\mathbf{k})(C_4^z)^{-1} = H(-k_y, k_x, k_z)$ with $C_4^z = e^{-i\frac{\pi}{4}\sigma_z}$. When $1 < |M/J| < 3$, the Hamiltonian represents a strong topological insulator with odd number of Dirac points in the energy spectra of surface states; when $|M/J| < 1$, it describes a weak topological insulator with even number of Dirac points in the surface energy spectra [88, 89].

To generate the higher-order topological insulating phase, Ref. [50] introduces the term involving Δ_2 that breaks both the time-reversal symmetry and the rotational symmetry but preserves the symmetry of their product, i.e., $C_4^z \mathcal{T}$. This term provides an effective mass, opening the gap of the Dirac points on the surface vertical to either x or y axis. Since the signs of the Dirac masses are opposite for neighboring surfaces, the hinges of their intersections exhibit chiral modes, similar to the chiral modes of a Chern insulator. It has been found that four chiral modes exist on the four hinges between the surfaces normal to x and y axes. The topological property of this higher-order phase can be characterized by the Chern-Simons term

$$\theta = \frac{1}{4\pi} \int d^3k \epsilon_{abc} \text{tr}[\mathcal{A}_a \partial_b \mathcal{A}_c + i\frac{2}{3} \mathcal{A}_a \mathcal{A}_b \mathcal{A}_c], \quad (2)$$

where $\mathcal{A}_{a;n,n'} = i \langle \varphi_n(\mathbf{k}) | \partial_{k_a} | \varphi_{n'}(\mathbf{k}) \rangle$ with $a, b, c \in \{x, y, z\}$ is the k_a -component of Berry connection, $|\varphi_n(\mathbf{k})\rangle$ is the Bloch eigenstate of $H_L(\mathbf{k})$ and n, n' are running over the occupied bands of the system. The topological invariant is quantized to 0 or π by $C_4^z \mathcal{T}$ symmetry [50].

For simplicity without loss of generality, we set $\Delta_1 = \Delta_2 = J$. In Fig. 1, we plot the energy spectra in a geometry with open boundaries along x and y and periodic boundaries along z . We see that there exist chiral modes

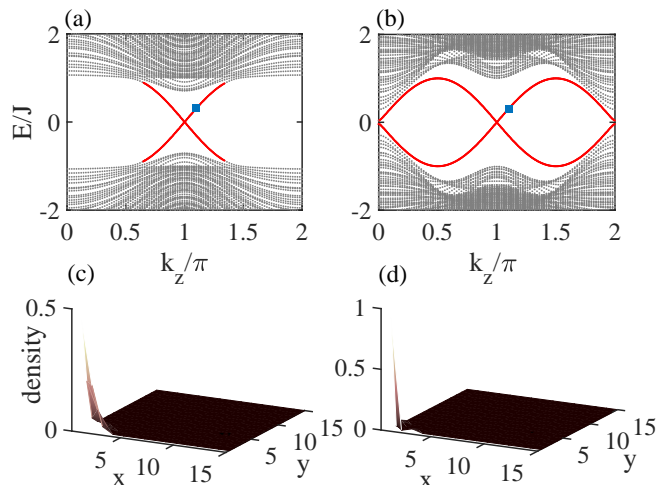


FIG. 1. Energy spectra with respect to k_z for a system with open boundaries along x and y and periodic boundary along z for (a) $M = 2J$ and (b) $M = 0.8J$, corresponding to strong and weak topological insulators, respectively, when $\Delta_2 = 0$. The red lines depict the states localized on the four hinges. The hinge modes are chiral in the former case but not in the latter. The density profiles of a hinge mode in the (x, y) plane for (a) $M = 2J$ and $k_z = 8\pi/7$ and (b) $M = 0.8J$ and $k_z = 8\pi/7$, characterized by the density distribution in the (x, y) plane, $\sum_{\lambda=1,2,3,4} |\varphi_{k_z, \lambda}(x, y)|^2$, where φ_{k_z} is the eigenstate corresponding to the eigenenergy labelled by the blue squares in (a-b) of the Hamiltonian (1) with open boundaries along the x and y directions and periodic boundary along the z direction, i.e., $H_L(k_z)\varphi_{k_z} = \varepsilon_{k_z}\varphi_{k_z}$. Here $\Delta_1 = \Delta_2 = J$.

localized on the hinges when $M = 2J$ in the strong topological regime. When $M = 0.8J$ in the weak topological regime, we can still observe the hinge-localized modes, but they are not chiral. We find solitons in both of these two cases, but their stabilities manifested by time evolution are different, which will be discussed in detail in the following.

III. HINGE SOLITONS

To create the hinge solitons, we add nonlinear terms into the higher-order topological system so that the dynamics is governed by the following nonlinear Schrödinger equation,

$$i\hbar \frac{\partial \psi(\mathbf{r}, t)}{\partial t} = [H_L + H_N(\psi)] \psi(\mathbf{r}, t), \quad (3)$$

where $H_N(\psi)_{(\mathbf{r}, \lambda), (\mathbf{r}', \lambda')} = \delta_{\mathbf{r}\mathbf{r}'} \delta_{\lambda\lambda'} g_\lambda |\psi_\lambda(\mathbf{r})|^2$ represents the short-range nonlinear interactions with g_λ denoting their strength for each component, H_L is the real space counterpart of the Hamiltonian (1) and $\psi(\mathbf{r}, t)$ is the wave function. Here we consider a cubic local nonlinear interaction, which widely exists in ultracold atoms and nonlinear optics [2, 90]. For simplicity, we set $g_\lambda = g > 0$.

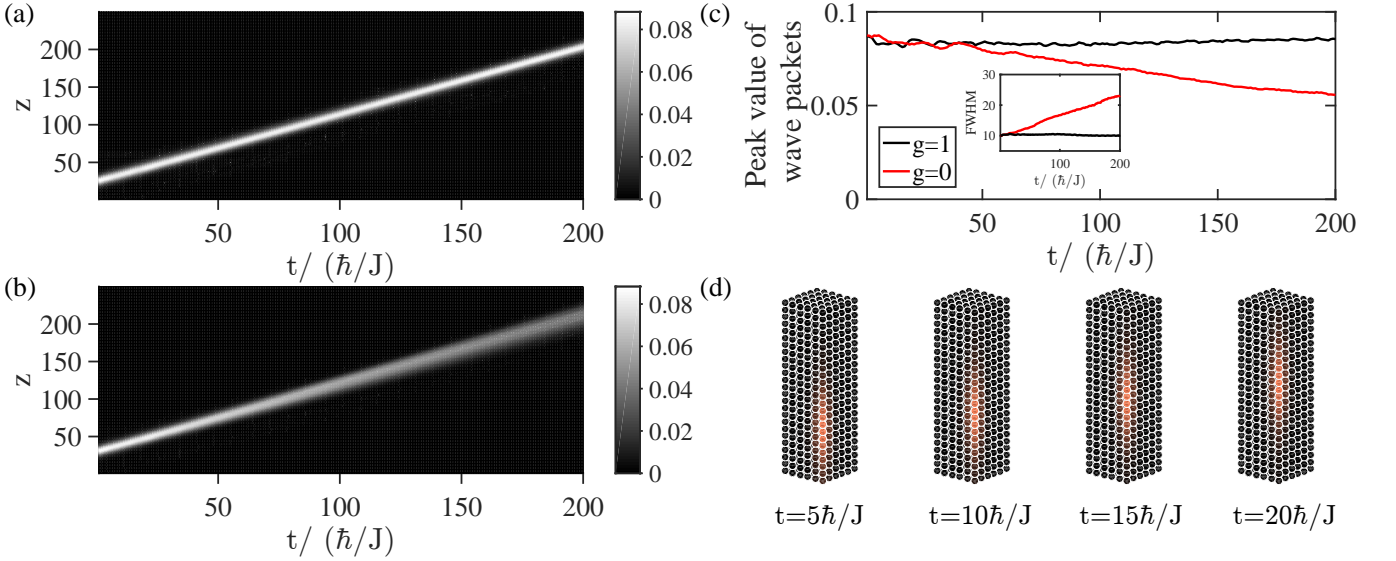


FIG. 2. The time evolution of a wave packet characterized by $\sum_{\lambda=1,2,3,4} |\psi_{\lambda}|^2$ for (a) $g = J$ and (b) $g = 0$. The wave packet is initialized at $t = 0$ based on Eq. (5) and Eq. (8) with $k_z = 8\pi/7$, $\varepsilon'' = -0.4374$ and $\delta = 0.007J$. (c) The evolution of the peak value of wave packets over time with the black and red lines denoting the cases with $g = J$ and $g = 0$, respectively. The inset plots the change of the full width at half maximum (FWHM) of the wave packets as time evolves. (d) Visualization of the propagation of the soliton over time in real space. See also the supplementary material for the dynamics of a soliton when it enters into the top surface. Here $M = 2J$.

Following Ref. [91], we construct a wave packet using the hinge modes of H_L to determine a soliton solution,

$$\psi_{\lambda}(\mathbf{r}, t) = \int_{-\pi}^{\pi} a(\kappa, t) \varphi_{k_z + \kappa, \lambda}(x, y) e^{-i\varepsilon_{k_z + \kappa} t + i(k_z + \kappa)z} d\kappa, \quad (4)$$

where $\lambda = 1, 2, 3, 4$ is the component index, φ_{k_z} denotes the hinge mode of $H_L(k_z)$ corresponding to the eigenenergy ε_{k_z} and $a(\kappa, t)$ denotes the weights for the corresponding hinge mode over time.

We now apply the Taylor-series expansion in κ for $\varphi_{k_z + \kappa, \lambda}(x, y)$ in the above integral to simplify Eq. (4) to

$$\psi_{\lambda}(\mathbf{r}, t) = e^{-i\varepsilon_{k_z} t + ik_z z} \sum_{j=0}^{\infty} \frac{(-i)^j}{j!} \frac{\partial^j \varphi_{k_z, \lambda}}{\partial k_z^j} \frac{\partial^j a(z, t)}{\partial z^j}, \quad (5)$$

where $a(z, t) = \int_{-\pi}^{\pi} a(\kappa, t) e^{i\kappa z} d\kappa$ is the envelope function of the corresponding soliton. Applying H_L to the wave function ψ in Eq. (5) and then performing the Taylor-series expansion for both $\varepsilon_{k_z + \kappa}$ and $\varphi_{k_z + \kappa, \lambda}(x, y)$ yields

$$H_L \psi = e^{-i\varepsilon_{k_z} t + ik_z z} \sum_{j=0}^{\infty} \frac{(-i)^j}{j!} \frac{\partial^j (\varepsilon_{k_z} \varphi_{k_z})}{\partial k_z^j} \frac{\partial^j a(z, t)}{\partial z^j}. \quad (6)$$

Suppose that φ_{k_z} varies much more slowly with respect to k_z than ε_{k_z} , we can make the approximation that $\partial^j (\varepsilon \varphi) / \partial k_z^j \approx \varphi \partial^j \varepsilon / \partial k_z^j$. By further assuming that $a(z, t)$ varies slowly in time and space, we obtain an approximate nonlinear Schrödinger equation for the envelop

function

$$i \frac{\partial a}{\partial t} + i\varepsilon' \frac{\partial a}{\partial z} + \frac{\varepsilon''}{2} \frac{\partial^2 a}{\partial z^2} - g_{\text{eff}} |a|^2 a = 0, \quad (7)$$

where $\varepsilon' = \partial \varepsilon_{k_z} / \partial k_z$, $\varepsilon'' = \partial^2 \varepsilon_{k_z} / \partial k_z^2$ and $g_{\text{eff}} = g \sum_{x, y, \lambda} |\varphi_{k_z, \lambda}(x, y)|^4$. Evidently, this equation is exactly the same as the Gross-Pitaevskii equation for a BEC in a free space in a reference moving with the velocity of $-\varepsilon'$ with $1/\varepsilon''$ playing the role of an effective mass. If $g_{\text{eff}} = 0$, this equation does not support a localized solution. Because of the chiral property of the hinge modes in the strong regime, the solitons can only move along one direction on a hinge, which is fundamentally different from solitons in a one-dimensional system whose velocities can be either positive or negative.

When $\varepsilon'' < 0$ for $g_{\text{eff}} > 0$, this equation has a bright soliton solution with a density peak,

$$a_B(z, t) = (2\delta/g_{\text{eff}})^{1/2} \text{sech} \left[(-2\delta/\varepsilon'')^{1/2} (z - \varepsilon' t) \right] e^{-i\delta t}, \quad (8)$$

where $\delta > 0$ describes the energy difference between the nonlinearity-induced energy eigenvalue μ and the linear one ε_{k_z} at k_z . While the Eq. (8) supports solutions for any positive value of δ , δ cannot be too large for a hinge soliton solution. On the one hand, the width of the soliton decreases as δ increases, meaning that if δ is very large, the width is very small so that we can not apply the approximation that the wave packet varies slowly in space. On the other hand, for large δ , $\mu = \varepsilon_{k_z} + \delta$ can be moved into the bulk energy spectra, resulting in the scattering of the soliton into the

bulk states. For a BEC, the total atom number N is given by $\sum_{\lambda} \int |\psi_{\lambda}(\mathbf{r})|^2 d\mathbf{r} = N$. For clarity, if we consider a zero-order approximation based on Eq. (5) so that $\psi_{\lambda}(\mathbf{r}, t) \approx e^{-i\varepsilon_{k_z} t + ik_z z} \varphi_{k_z, \lambda} a_B(z, t)$, the atom number constraint yields $\int |a_B(z, t)|^2 dz = N$. We thus obtain $\delta = -\frac{g_{eff}^2 N^2}{8\varepsilon''}$, showing that the bright soliton becomes narrower with its peak value being increased as we increase g with N being fixed.

To show that a bright soliton localized on a hinge can exist in the second-order topological insulator, we now study the dynamics of the soliton by solving the nonlinear Schrödinger equation numerically. We first construct an initial wave packet using the hinge modes in the strong topological insulator based on Eqs. (5) and (8) and then observe the dynamics of the wave packet as time evolves. Fig. 2(a) illustrates that the wave packet moves unidirectionally along the z axis without changing its shape with the velocity determined by ε' , implying the existence of a travelling soliton. In comparison, we also calculate the dynamics of the same initial wave packet in the linear case with $g = 0$ (without nonlinearities) and plot the results in Fig. 2(b). The figure shows that the wave packet diffuses significantly as time progresses. The diffusion of the wave packet happens in the linear scenario because the hinge spectrum is not perfectly linear. To show the difference quantitatively, we further compare the time evolution of the maximum value and the full width at half maximum of the wave packet for these two cases in Fig. 2(c). We can see clearly that in the nonlinear case, the peak value becomes stable after some slight oscillations, whereas in the linear case, it suffers a continuous decline. The propagation of the hinge soliton over time is also visually displayed in Fig. 2(d). The above analysis demonstrates the existence of a stable bright hinge soliton in the second-order topological insulator.

When $\varepsilon'' > 0$ for $g_{eff} > 0$, Eq. (7) allows for the existence of the following dark soliton solution with a density dip,

$$a_D(z, t) = (\delta/g_{eff})^{1/2} \tanh[(\delta/\varepsilon'')^{1/2}(z - \varepsilon't)] e^{-i\delta t}. \quad (9)$$

For a BEC with a fixed atom number, similar to the case of the bright soliton, if we consider atoms trapped in a cubic box with size $L \gg 1$, then we obtain an expression of δ in terms of g_{eff} and N , i.e., $\delta = [\frac{\sqrt{\varepsilon''}}{L} + \sqrt{\frac{\varepsilon''}{L^2} + \frac{Ng_{eff}}{L}}]^2$. It indicates that the dark soliton becomes narrower when g is increased. To numerically demonstrate the dynamics of the dark soliton, we first construct an initial wave packet with a density dip based on Eqs. (5) and (9) and then compute the dynamics of the wave packet. Fig. 3 illustrates that the wave packet travels along z with its dip shape remaining almost unchanged during the time evolution. This demonstrates that a dark soliton can stably exist on the hinges in the second-order topological insulator.

In the strong topological regime when $1 < |M/J| < 3$, there are chiral hinge modes in the energy gap. In contrast, in the weak topological regime when $|M/J| < 1$,

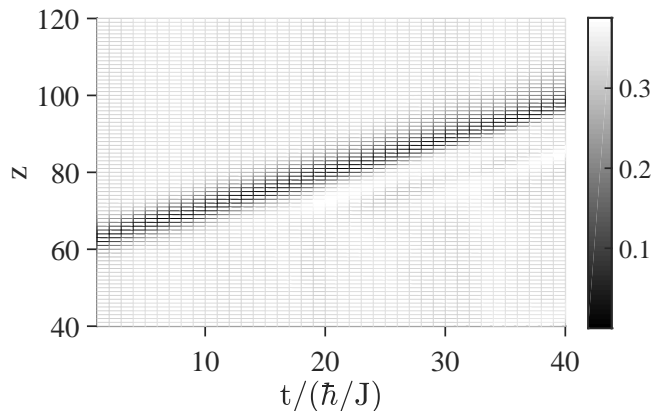


FIG. 3. The propagation of a wave packet over time, showing the existence of a dark soliton. The wave packet is initialized at $t = 0$ based on Eq. (5) and Eq. (9) with $k_z = 6\pi/7$, $\varepsilon'' = 0.4374$ and $\delta = 0.07J$. Here $M = 2J$.

instead of being chiral for the hinge modes, there are two states with opposite group velocities on each hinge for each energy in the energy gap [see Fig. 1(b)]. We now apply the same method to explore whether a stable bright soliton can exist on a hinge of a weak second-order topological insulator. Similar to the strong topological case, we find that the wave packet travels steadily along z without noticeable change of its shape, suggesting the existence of a stable bright soliton. But the soliton gradually slows down over time as shown in Fig. 4, possibly due to the scattering of the state to other modes with the same energy and opposite group velocity. In comparison, we also plot the velocity of the soliton with respect to time for the former case with $M = 2J$ in Fig. 4, showing that the velocity remains stable. While the figure shows a very small decline of the velocity, it may be caused by the numerical error, as the decline becomes smaller when we use a smaller step size of time in the computation. Note that this numerical error in the latter case with $M = 0.8J$ also exists but is not as noticeable as in the former one.

IV. HINGE SOLITONS IN ELECTRIC CIRCUITS

In this section, we will introduce a practical scheme to realize the second-order topological insulator in 3D and demonstrate that a bright soliton for the voltage distribution can exist in the presence of nonlinear inductors.

Let us now consider an electric network with a number of nodes labelled by m . Suppose that an electric current I_m is externally flowing into node m and the current then flows into other nodes, which are connected with node m . According to Kirchhoff's law, we have

$$I_m = \sum_n I_{mn} = \sum_n Y_{mn}(V_m - V_n) + Y_m V_m, \quad (10)$$

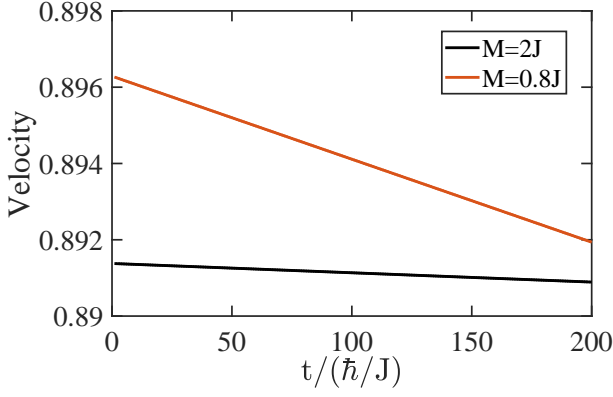


FIG. 4. The change of a soliton's velocity as time evolves. The soliton is initialized at $t = 0$ based on Eq. (5) and Eq. (8) with $k_z = 8\pi/7$ and $\delta = 0.007J$. The black and red lines depict the scenarios with $M = 2J$ and $M = 0.8J$, respectively. Here the step size of time is $\Delta t = 1 \times 10^{-3} \hbar/J$.

where I_{mn} denotes the current flowing from node m to node n , Y_{mn} and Y_m represent the admittance between node m and node n and the admittance between node m and the ground, respectively, and V_m denotes the voltages measured at node m against ground. The relation above can be written in a matrix form as

$$I = LV, \quad (11)$$

where L is the Laplacian with $L_{mn} = -Y_{mn} + \delta_{mn}(Y_m + \sum_n Y_{mn})$ and I and V are the column vectors consisting of electric currents and potentials at each node. Consider the alternating current with the frequency of ω_0 (i.e., $I = \mathcal{I}e^{i\omega_0 t}$ and $V = \mathcal{V}e^{i\omega_0 t}$), we have

$$\mathcal{I} = i\omega_0 \mathcal{L}(\omega_0) \mathcal{V}. \quad (12)$$

To simulate the Hamiltonian in Eq. (1), we need to engineer electric connections so that $\mathcal{L} = H_L$ where H_L is the real space Hamiltonian of $H_L(\mathbf{k})$ in Eq. (1). Since there are four degrees of freedom in each unit cell, we consider four nodes in each unit cell as shown in Fig. 5(a). Evidently, inductors and capacitors between two neighboring nodes contribute terms corresponding to the hopping with positive and negative amplitude, respectively. For the hopping with imaginary amplitudes, we utilize negative impedance converters with current inversion (INICs) [81], whose structure is shown in Fig. 5(a). Its node voltage equation is

$$\mathcal{I}_N = \frac{1}{R} \begin{bmatrix} -v & v \\ -1 & 1 \end{bmatrix} \mathcal{V}_N, \quad (13)$$

where $\mathcal{I}_N = (\mathcal{I}_1 \ \mathcal{I}_2)^T$, $\mathcal{V}_N = (\mathcal{V}_1 \ \mathcal{V}_2)^T$ and $v = R_b/R_a$ (consider $v = 1$ here) as shown in Fig. 5(a). Clearly, when the current flows following the direction of the INIC (the large arrow), the resistance is negative and it is positive, when the direction is opposite.

TABLE I. Configurations for the electric element denoted by a circle labelled by G in Fig. 5(a) for different positions for a system in a geometry with open boundaries in the (x, y) plane with $N_x \times N_y$ unit cells and periodic boundaries along z . The units of capacitors, inductors and INICs are J_E , $1/(\omega_0^2 J_E)$ and $1/(\omega_0 J_E)$, respectively. The arrow indicates the direction of the INICs and the symbol / indicates that the INICs are not required.

Position	Elements		
	Capacitor	Inductor	INICs
Bulk	(6,6,3,3)	$(\frac{1}{3}, \frac{1}{3}, \frac{1}{6}, \frac{1}{6})$	(/,/,/,/)
$(x, y) = (1, 1)$	(6.5,6.5,5,5)	$(\frac{1}{5}, \frac{1}{5}, \frac{1}{6.5}, \frac{1}{6.5})$	($\downarrow, \uparrow, \uparrow, \downarrow$)
$(x, y) = (N_x, 1)$	(7,7,4.5,4.5)	$(\frac{1}{4.5}, \frac{1}{4.5}, \frac{1}{7}, \frac{1}{7})$	($\downarrow, \uparrow, \uparrow, \downarrow$)
$(x, y) = (1, N_y)$	(6.5,6.5,5,5)	$(\frac{1}{5}, \frac{1}{5}, \frac{1}{6.5}, \frac{1}{6.5})$	($\uparrow, \downarrow, \downarrow, \uparrow$)
$(x, y) = (N_x, N_y)$	(7,7,4.5,4.5)	$(\frac{1}{4.5}, \frac{1}{4.5}, \frac{1}{7}, \frac{1}{7})$	($\uparrow, \downarrow, \downarrow, \uparrow$)
Surface($y = 1$)	(6.5,6.5,4,4)	$(\frac{1}{3.5}, \frac{1}{3.5}, \frac{1}{6}, \frac{1}{6})$	($\downarrow, \uparrow, \uparrow, \downarrow$)
Surface($y = N_y$)	(6.5,6.5,4,4)	$(\frac{1}{3.5}, \frac{1}{3.5}, \frac{1}{6}, \frac{1}{6})$	($\uparrow, \downarrow, \downarrow, \uparrow$)
Surface($x = 1$)	(6,6,4,4)	$(\frac{1}{4.5}, \frac{1}{4.5}, \frac{1}{6}, \frac{1}{6})$	(/,/,/,/)
Surface($x = N_x$)	(6.5,6.5,3.5,3.5)	$(\frac{1}{4}, \frac{1}{4}, \frac{1}{7}, \frac{1}{7})$	(/,/,/,/)

The scheme shown in Fig. 5 realizes a Laplacian that simulates the Hamiltonian in Eq. (1) [i.e., $\mathcal{L}(\omega_0) = H_E(\omega_0)$] with

$$H_E(\omega_0) = (M_E + J_E \sum_{\nu=x,y,z} \cos k_\nu) \tau_z \quad (14)$$

$$+ \Delta_{E1} \sum_{\nu=x,y,z} \sin k_\nu \tau_y \sigma_\nu + \Delta_{E2} (\cos k_x - \cos k_y) \tau_x,$$

when $J_C = J_E/2$, $J_L = 2/(\omega_0^2 J_E)$, $\Delta_{1C} = \Delta_{E1}/2$, $\Delta_{1L} = 2/(\omega_0^2 \Delta_{E1})$, $\Delta_{2C} = \Delta_{E2}/2$, $\Delta_{2L} = 2/(\omega_0^2 \Delta_{E2})$, and $1/(\omega_0^2 M_L) = M_C = M_E$. This Hamiltonian takes the same form as Eq. (1) after a transformation: $\tau_x \rightarrow \tau_y$ and $\tau_y \rightarrow \tau_x$ which doesn't affect topological properties of the system. For simplicity, we set $\Delta_{E1} = \Delta_{E2} = J_E$. In the scheme, the connections inside each layer (the connections between distinct layers) are displayed in Fig. 5(c) [Fig. 5(d)] with detailed electric structures shown in Fig. 5(e). In each unit cell, there are four nodes connected to the ground with electric elements contributing to the diagonal terms. The electric element denoted by a circle labelled by G is employed to cancel the diagonal entries contributed by the electric elements connecting two distinct nodes. Explicit configurations for the elements are listed in Table (I). Additional linear inductors and capacitors are used to generate the mass term. This electric circuit can be utilized to study the topological properties of the second-order topological insulator in 3D if the nonlinear inductor is not involved.

To simulate the dynamics of a soliton, we solve the following equation of motion of the circuit [81]

$$\frac{d}{dt} I(t) = \mathcal{C} \frac{d^2}{dt^2} V(t) + \Sigma \frac{d}{dt} V(t) + \Pi V(t) \quad (15)$$

where \mathcal{C} , Σ , and Π are the real-valued matrices characterizing the capacitance of capacitors, the conductance of the INICs, and the inductance of inductors, respectively..

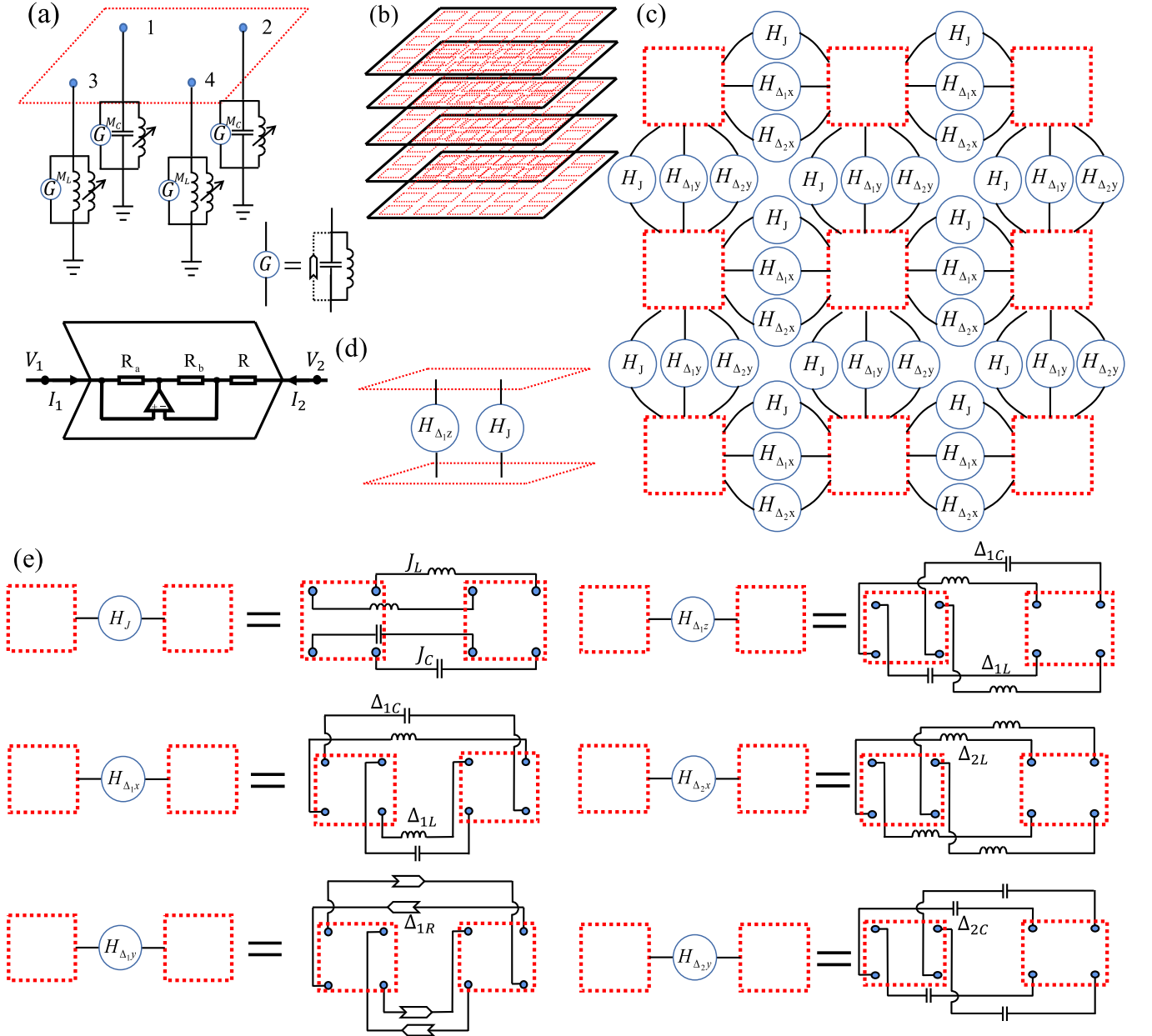


FIG. 5. (a) Schematics of a unit cell consisting of four nodes, each of which is connected to some grounded electric elements to simulate the diagonal entries in the Hamiltonian and nonlinear terms in H_N . The electric element denoted by a circle labelled by G is used to cancel the diagonal entries contributed by the electric elements connecting two distinct nodes. The specific configurations for these elements are listed in Table I. The detailed structure of the INIC is displayed in the lower part. (b) Scheme of an electric circuit for simulation of the second-order topological insulator in 3D. The connection inside each layer [in the (x, y) plane] is shown in (c) and the connection between different layers along z is shown in (d). (e) The detailed electric structure for the circles labelled by H_J , $H_{\Delta_{1\nu}}$ ($\nu = x, y, z$) and $H_{\Delta_{2\nu}}$ ($\nu = x, y$) in (c) and (d). J_L , Δ_{1L} and Δ_{2L} denote the inductances of the corresponding inductors, J_C , Δ_{1C} and Δ_{2C} denote the capacitances of the corresponding capacitors, and Δ_{1R} denotes the resistance of the INIC (corresponding to R in the lower part of (a)).

These matrices in momentum space are given by

$$\mathcal{C}(\mathbf{k}) = A_C + M\tau_z - 2J_C \sum_{\nu=x,y,z} \cos k_\nu (\tau_0 - \tau_z)/2 - 2\Delta_{2C} \cos k_y \tau_x - \Delta_{1C} \cos k_x \tau_x \sigma_x - \Delta_{1C} \cos k_z \tau_x + \Delta_{1C} \sin k_x \tau_y \sigma_x + \Delta_{1C} \sin k_z \tau_y \sigma_z \quad (16)$$

$$\Sigma(\mathbf{k}) = \frac{2}{\Delta_{1R}} \sin k_y \tau_y \sigma_y \quad (17)$$

$$\begin{aligned} \Pi(\mathbf{k}) = & A_L - \frac{2}{J_L} \sum_{\nu=x,y,z} \cos k_\nu (\tau_0 + \tau_z)/2 \\ & - \frac{2}{\Delta_{2L}} \cos k_x \tau_x - \frac{1}{\Delta_{1L}} (\cos k_x \tau_x \sigma_x + \sin k_x \tau_y \sigma_x) \\ & - \frac{1}{\Delta_{1L}} (\cos k_z \tau_x + \sin k_z \tau_y \sigma_z), \end{aligned} \quad (18)$$

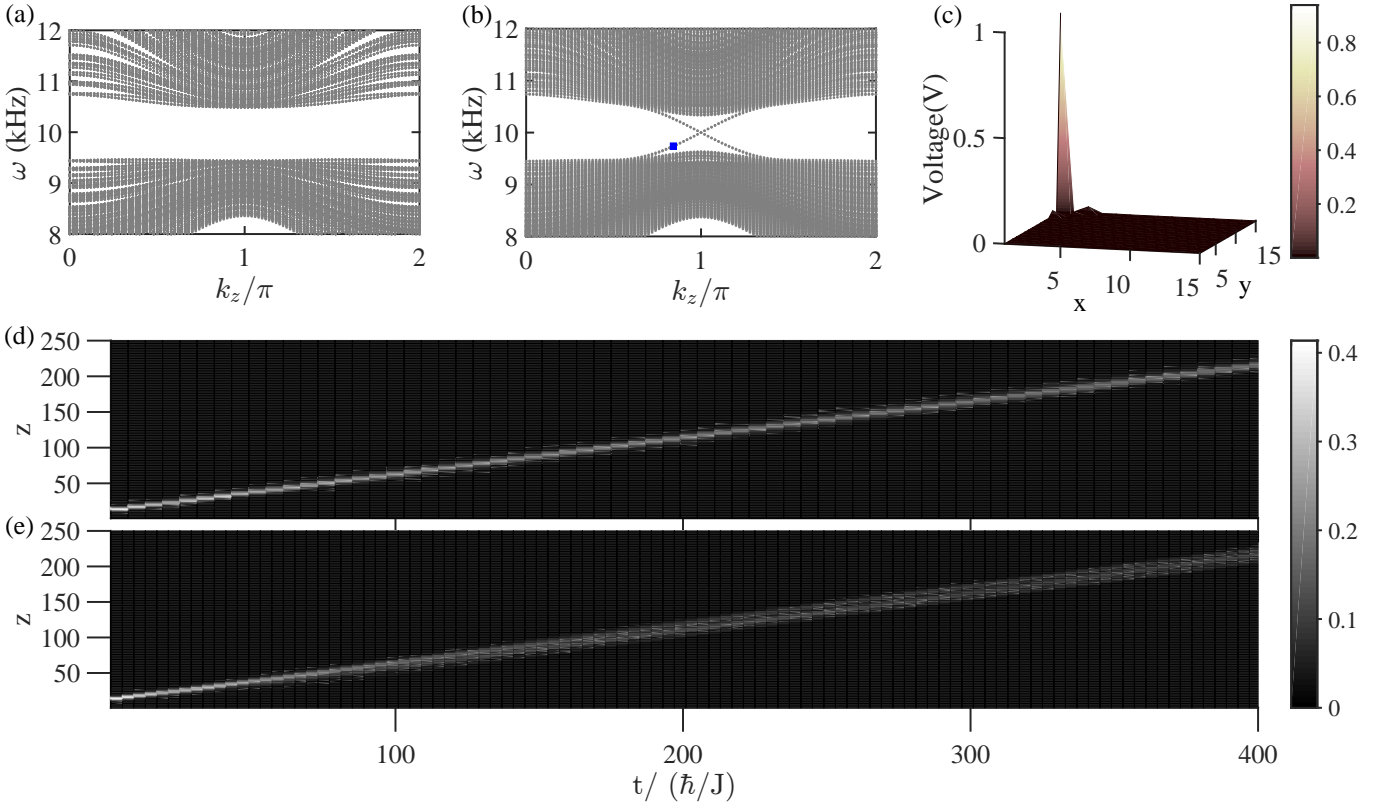


FIG. 6. The eigenfrequency spectra versus momentum k_z of H_{HTIC} with (a) periodic boundaries and (b) open boundaries along x and y . Note that only positive parts of the spectra are plotted. The lines traversing the gap describe the hinge-localized states. (c) The voltage distribution of a hinge mode of H_{HTIC} in the (x, y) plane at $k_z = 6\pi/7$, described by $\sqrt{\sum_{\lambda=5,6,7,8} \phi_{k_z, \lambda}(x, y)^2}$, where $\phi_{k_z}(x, y)$ is the eigenvector of H_{HTIC} corresponding to the eigenfrequency labelled by the blue squares in (b) of H_{HTIC} with open boundaries along x and y and periodic boundary along z . The time evolution of a voltage pulse characterized by $\sqrt{\sum_{\lambda=5,6,7,8} |\Psi_\lambda(t)|^2}$ for (d) $g_c = 10 \text{ mH}^{-1} \text{V}^{-2}$ and (e) $g_c = 0$. The voltage pulse is initialized at $t = 0$ to the state described by Eq. (26) with $a_0 = 1$, $\lambda_0 = 0.5$ and $k_z = 6\pi/7$. Here $\Delta_{1C} = \Delta_{2C} = J_C = 50 \mu\text{F}$, $\Delta_{1L} = \Delta_{2L} = J_L = 200 \mu\text{H}$, $\Delta_{2R} = 2 \Omega$, and $M_C = 100 \mu\text{F}$.

where $A_C + M\tau_z$ and A_L are contributed by the grounded capacitors and inductors, respectively. When $J_C = \Delta_{1C}$ and $J_L = \Delta_{1L}$ without M_C and M_L , we have $A_C = 8J_C$, $M = 2J_C$, and $A_L = 8/\Delta_{1L}$ using the grounding configurations listed in Table I.

For alternating input currents with the frequency of ω [$I(t) = \mathcal{I}e^{i\omega t}$ and $V(t) = \mathcal{V}e^{i\omega t}$], this differential equation gives rise to the circuit Laplacian

$$L(\omega) = i\omega\mathcal{C} + \Sigma + \frac{1}{i\omega}\Pi = i\omega\mathcal{L}(\omega) \quad (19)$$

so that $\mathcal{I} = L(\omega)\mathcal{V}$, which is the same as Eq. (12).

Let us now consider a specific case without any input currents, i.e., $I(t) = 0$. In this case, we reduce the Eq. (15) to the following first-order differential equation similar to the Schrödinger equation for the higher-order topological insulator circuit (HTIC),

$$-i\frac{d}{dt}\Psi = H_{\text{HTIC}}\Psi, \quad (20)$$

where $\Psi = (\dot{V}(t), V(t))^T$, and

$$H_{\text{HTIC}} = i \begin{bmatrix} \mathcal{C}^{-1}\Sigma & \mathcal{C}^{-1}\Pi \\ -1 & 0 \end{bmatrix}. \quad (21)$$

This differential equation has the solution of $\Psi(t) = e^{i\omega_n t}\phi_n$, where ϕ_n is an eigenvector of H_{HTIC} corresponding to the eigenvalue ω_n . Clearly, the eigenvalues of H_{HTIC} appear in pairs as $(\omega_n, -\omega_n^*)$. While H_{HTIC} is non-Hermitian, its eigenvalues are real due to the positive semidefinite properties of \mathcal{C} and Π [81], implying that the eigenvalues emerge in pairs as $(\omega_n, -\omega_n)$.

Since ω_n is the alternating current frequency allowed by Eq. (20), we must have $L(\omega_n)\mathcal{V} = 0$ given that the input currents are zero. To have nontrivial solutions, we require $\det(L(\omega_n)) = 0$. In other words, there exist eigenvectors V_n of $L(\omega_n)$ with zero eigenvalue, i.e.,

$$L(\omega_n)V_n = 0. \quad (22)$$

One can change the equation into the following form

$$H_{\text{HTIC}}\phi_n = \omega_n\phi_n, \quad (23)$$

where

$$\phi_n = (i\omega_n V_n \quad V_n)^T. \quad (24)$$

It also tells us that if $L(\omega_n)$ has zero eigenvalues, then ω_n is an eigenvalue of H_{HTIC} .

The intimate connection suggests that the band structures of H_{HTIC} and $H_E(\omega_0) = \mathcal{L}(\omega_0)$ share some common properties. For example, if $H_E(\omega_0)$ is in a higher-order topological phase with chiral hinge modes, then there exist four zero-energy hinge modes at $k_z = \pi$ [see Fig. 1(a)]. Based on the discussion above, ω_0 should be an eigenvalue of H_{HTIC} . In addition, according to Eq. (24), we have four modes of H_{HTIC} with frequency of ω_0 localized on the hinges, suggesting that H_{HTIC} has chiral hinge modes. Indeed, Fig. 6(b) illustrates that H_{HTIC} exhibits the chiral hinge modes across the gap, which do not exist for periodic boundaries along x and y [see Fig. 6(a)]. The voltage distribution of these states also shows that they are localized on the hinges [see Fig. 6(c)]. We note that gapless nontrivial states in circuits have also been found in other 2D systems [67, 81].

In stark contrast to a soliton for the atomic density in BECs, in our case, a soliton is for the voltage distribution in the electric circuit. To generate the soliton, we add nonlinear inductors in the circuit, which may be realized by a voltage-controlled variable inductor [92, 93]. Each nonlinear inductor connects each node with the ground (see Fig. 5), contributing a nonlinear inductance described by

$$\Pi_{N(\mathbf{r},\lambda),(\mathbf{r}',\lambda')} = g_c \delta_{\mathbf{r}\mathbf{r}'} \delta_{\lambda\lambda'} |V_{\mathbf{r},\lambda}|^2, \quad (25)$$

where $V_{\mathbf{r},\lambda}$ denotes the voltage at the node labelled by \mathbf{r}, λ .

To create a bright soliton, we initialize the state at $t = 0$ as

$$\Psi(\mathbf{r}, t = 0) = a_0 \text{sech}(\lambda_0 z) e^{ik_z z} \phi_{k_z}(x, y), \quad (26)$$

and then observe its dynamics. Here a_0 and λ_0 are real parameters and $\phi_{k_z}(x, y)$ is a hinge mode of H_{HTIC} for a quasimomentum of k_z in a geometry with open boundaries along x and y and periodic boundary along z . To simulate the dynamics, we impose open boundary conditions along all directions, in which case the parameters of the grounding elements at the corners and on the

surface perpendicular to the z axis need to be adjusted to cancel the diagonal parts contributed by the electric elements connecting distinct nodes. For a specific example with $g_c = 10\text{mH}^{-1}\text{V}^{-2}$, $k_z = 6\pi/7$, $\Delta_{1C} = \Delta_{2C} = J_C = 50\ \mu\text{F}$, $\Delta_{1L} = \Delta_{2L} = J_L = 200\ \mu\text{H}$, $\Delta_{2R} = 2\ \Omega$, and $M_C = 100\ \mu\text{F}$, we take $a_0 = 1$ and $\lambda_0 = 0.5$. In Fig. 6(d) and (e), we plot the dynamics of the voltage peak with and without nonlinearity, respectively. It can be seen that the voltage distribution with nonlinearity is stable without conspicuous dispersion as time evolves. In stark contrast, in the case without nonlinearity, the wave packet for the voltage distribution becomes wider as it evolves over time. This shows the existence of a hinge bright soliton in the nonlinear circuit system.

V. CONCLUSION

In summary, we have theoretically studied solitons in a 3D second-order topological insulator when nonlinearity is involved. We find that solitons can exist in both the strong and weak regimes, but the soliton in the former regime is more stable than that in the latter regime given that the latter one gradually slows down as time progresses. In addition, the soliton on a hinge in the strong regime can only move along one direction due to the chiral property of hinge modes. To realize the soliton in a practical experimental system, we further introduce an electric network to simulate the 3D second-order topological insulator. By calculating the dynamics of a voltage pulse in the electric circuit, we show the existence of a soliton for the voltage distribution when nonlinear inductors are involved. Such solitons can also be experimentally observed in other nonlinear systems, such as ultracold atomic gases and nonlinear optics.

ACKNOWLEDGMENTS

This work is supported by the start-up fund from Tsinghua University, the National Thousand-Young-Talents Program and the National Natural Science Foundation of China (11974201).

-
- [1] Kivshar Y S and Agrawal G P 2003 *Optical solitons* (San Diego: Academic Press)
- [2] Dauxois T and Peyrard M 2006 *Physics of Solitons* (Cambridge: Cambridge University Press)
- [3] Zeng L and Zeng J 2020 Preventing critical collapse of higher-order solitons by tailoring unconventional optical diffraction and nonlinearities *Commun. Phys.* **3**, 26
- [4] Shabat A and Zakharov V 1972 Exact theory of two-dimensional self-focusing and one-dimensional self-modulation of waves in nonlinear media *Sov. Phys. JETP.* **34** 62
- [5] Burger S, Bongs K, Dettmer S, Ertmer W, Sengstock K, Sanpera A, Shlyapnikov G V and Lewenstein M 1999 Dark Solitons in Bose-Einstein Condensates *Phys. Rev. Lett.* **83** 5198
- [6] Kevrekidis P G, Frantzeskakis D J and Carretero-González R 2007 *Emergent Nonlinear Phenomena in Bose-Einstein Condensates* (Springer)

- [7] Kartashov Y V, Konotop V V, Modugno M and Sherman E Ya 2019 Solitons in Inhomogeneous Gauge Potentials: Integrable and Nonintegrable Dynamics *Phys. Rev. Lett.* **122**, 064101
- [8] Zeng L and Zeng J 2019 Gap-type dark localized modes in a Bose-Einstein condensate with optical lattices *Adv. Photonics* **1**, 046006
- [9] Dziarmaga J and Sacha K 2005 Gap soliton in superfluid Fermi gas at zero and finite temperature *Laser Phys.* **15** 674-678
- [10] Antezza M, Dalfovo F, Pitaevskii L P and Stringari S 2007 Dark solitons in a superfluid Fermi gas *Phys. Rev. A* **76** 043610
- [11] Yefsah T, Sommer A T, Ku M J H, Cheuk L W, Ji W J, Bakr W S and Zwierlein M W 2013 Heavy solitons in a fermionic superfluid *Nature (London)* **499** 426
- [12] Xu Y, Mao L, Wu B and Zhang C 2014 Dark Solitons with Majorana Fermions in Spin-Orbit-Coupled Fermi Gases *Phys. Rev. Lett.* **113** 130404
- [13] Ku M J H, Ji W J, Mukherjee B, GuardadoSanchez E, Cheuk L W, Yefsah T and Zwierlein M W 2014 Motion of a Solitonic Vortex in the BEC-BCS Crossover *Phys. Rev. Lett.* **113** 065301
- [14] Zou P, Brand J, Liu X J and Hu H 2016 Traveling majorana solitons in a low-dimensional spin-orbit-coupled fermi superfluid *Phys. Rev. Lett.* **117** 225302
- [15] Sulem C and Sulem P L 1999 *The Nonlinear Schroedinger Equations Self-Focusing and Wave Collapse* (New York: Springer)
- [16] Kartashov Y V, Astrakharchik G E, Malomed B A and Kivshar Y S 2019 Frontiers in multidimensional self-trapping of nonlinear fields and matter *Nat. Rev. Phys.* **1**, 185-197
- [17] Pedri P and Santos L 2005 Two-Dimensional Bright Solitons in Dipolar Bose-Einstein Condensates *Phys. Rev. Lett.* **95** 200404
- [18] Lahaye T, Menotti C, Santos L, Lewenstein M and Pfau T 2009 The physics of dipolar bosonic quantum gases *Rep. Prog. Phys.* **72** 126401
- [19] Zhang Y C, Zhou Z W, Malomed B A and Pu H 2015 Stable Solitons in Three Dimensional Free Space without the Ground State: Self-Trapped Bose-Einstein Condensates with Spin-Orbit Coupling *Phys. Rev. Lett.* **115** 253902
- [20] Kartashov Y V and Zezyulin D A 2019 Stable Multiring and Rotating Solitons in Two-Dimensional Spin-Orbit-Coupled Bose-Einstein Condensates with a Radially Periodic Potential *Phys. Rev. Lett.* **122**, 123201
- [21] Lumer Y, Plotnik Y, Rechtsman M C and Segev M 2013 Self-Localized States in Photonic Topological Insulators *Phys. Rev. Lett.* **111** 243905
- [22] Ablowitz M J, Curtis C W and Ma Y P 2014 Linear and nonlinear traveling edge waves in optical honeycomb lattices *Phys. Rev. A* **90** 023813
- [23] Ablowitz M J, Curtis C W and Ma Y P 2015 Adiabatic dynamics of edge waves in photonic graphene *2D Mater.* **2** 024003
- [24] Ablowitz M J and Ma Y P 2015 Strong transmission and reflection of edge modes in bounded photonic graphene *Opt. Lett.* **40** 4635
- [25] Leykam D and Chong Y D 2016 Edge Solitons in Nonlinear-Photonic Topological Insulators *Phys. Rev. Lett.* **117** 143901
- [26] Kartashov Y V and Skryabin D V 2016 Modulational instability and solitary waves in polariton topological insulators *Optica* **3** 1228
- [27] Gulevich D R, Yudin D, Skryabin D V, Iorsh I V and Shelykh I A 2017 Exploring nonlinear topological states of matter with exciton-polaritons: Edge solitons in kagome lattice *Sci. Rep.* **7** 1780
- [28] Ablowitz M J and Cole J T 2017 Tight-binding methods for general longitudinally driven photonic lattices: Edge states and solitons *Phys. Rev. A* **96** 043868
- [29] Snee D D J M and Ma Y P 2019 Edge solitons in a nonlinear mechanical topological insulator *Extreme Mechanics Letters* **30** 100487
- [30] Smirnova D A, Smirnov L A, Leykam D and Kivshar Y S 2019 Topological Edge States and Gap Solitons in the Nonlinear Dirac Model *Laser Photonics Rev.* **13** 1900223
- [31] Elyasi M, Sato K and Bauer G E W 2019 Topologically nontrivial magnonic solitons *Phys. Rev. B* **99** 134402
- [32] Pal R K, Vila J, Leamy M and Ruzzene M 2019 Amplitude-dependent topological edge states in nonlinear phononic lattices *Phys. Rev. E* **97** 032209
- [33] Ivanov S K, Kartashov Y V, Maczewsky L J, Szameit A and Konotop V V 2020 Edge Solitons in Lieb Topological Floquet Insulators *Opt. Lett.* **45** 1459
- [34] Ivanov S K, Kartashov Y V, Szameit A, Torner L and Konotop V V 2020 Vector Topological Edge Solitons in Floquet Insulators *ACS Photonics* **7** 735
- [35] Zhang Z, Wang R, Zhang Y, Kartashov Y V, Li F, Zhong H, Guan H, Gao K, Li F, Zhang Y and Xiao M 2020 Observation of edge solitons in photonic graphene *Nat. Commun.* **11**, 1902
- [36] Mukherjee S and Rechtsman M C 2020 Observation of Floquet solitons in a topological bandgap *Science* **368** 856
- [37] Shang C, Zheng Y L and Malomed B A 2018 Weyl solitons in three-dimensional optical lattices *Phys. Rev. A* **97** 043602
- [38] Sitte M, Rosch A, Altman E and Fritz L 2012 Topological Insulators in Magnetic Fields: Quantum Hall Effect and Edge Channels with a Nonquantized θ Term *Phys. Rev. Lett.* **108** 126807
- [39] Zhang F, Kane C L and Mele E J 2013 Surface State Magnetization and Chiral Edge States on Topological Insulators *Phys. Rev. Lett.* **110** 046404
- [40] Benalcazar W A, Bernevig B A and Hughes T L 2017 Quantized electric multipole insulators *Science* **357** 61
- [41] Slager R J, Rademaker L, Zaenen J and Balents L 2015 Impurity-bound states and Green's function zeros as local signatures of topology *Phys. Rev. B* **92** 085126
- [42] Xu Y, Xue R and Wan S 2017 Topological Corner States on Kagome Lattice Based Chiral Higher-Order Topological Insulator arXiv:1711.09202
- [43] Langbehn J, Peng Y, Trifunovic L, von Oppen F and Brouwer P W 2017 Reflection-Symmetric Second-Order Topological Insulators and Superconductors *Phys. Rev. Lett.* **119** 246401
- [44] Song Z, Fang Z and Fang C 2017 $(d - 2)$ -Dimensional Edge States of Rotation Symmetry Protected Topological States *Phys. Rev. Lett.* **119** 246402
- [45] Benalcazar W A, Bernevig B A and Hughes T L 2017 Electric multipole moments, topological multipole moment pumping, and chiral hinge states in crystalline insulators *Phys. Rev. B* **96** 245115
- [46] Ezawa M 2018 Higher-Order Topological Insulators and Semimetals on the Breathing Kagome and Pyrochlore Lattices *Phys. Rev. Lett.* **120** 026801

- [47] Serra-Garcia M, Peri V, Süsstrunk R, Bilal O R, Larsen T, Villanueva L G and Huber S D 2018 Observation of a phononic quadrupole topological insulator *Nature* **555** 342-345
- [48] Peterson C W, Benalcazar W A, Hughes T L and Bahl G 2018 A quantized microwave quadrupole insulator with topologically protected corner states *Nature* **555** 346-350
- [49] Geier M, Trifunovic L, Hoskam M and Brouwer P W 2018 Second-order topological insulators and superconductors with an order-two crystalline symmetry *Phys. Rev. B* **97** 205135
- [50] Schindler F, Cook A M, Vergniory M G, Wang Z J, Parkin S S P, Bernevig B A and Neupert T 2018 Higher-Order Topological Insulators, *Sci. Adv.* **4** eaat0346
- [51] Yan Z, Song F and Wang Z 2018 Majorana Corner Modes in a High-Temperature Platform *Phys. Rev. Lett.* **121** 096803
- [52] Schindler F, Wang Z, Vergniory M G, Cook A M, Murani A, Sengupta S, Kasumov A Y, Deblock R, Jeon S, Drozdov I, Bouchiat H, Guéron S, Yazdani A, Bernevig B A and Neupert T 2018 Higher-order topology in bismuth *Nat. Phys.* **14** 918-924
- [53] Imhof S, Berger C, Bayer F, Brehm J, Molenkamp L W, Kiessling T, Schindler F, Lee C H, Greiter M, Neupert T and Thomale R 2018 Topolectrical-circuit realization of topological corner modes *Nat. Phys.* **14** 925-929
- [54] Wang Q, Liu C C, Lu Y M and Zhang F 2018 High-temperature majorana corner states *Phys. Rev. Lett.* **121** 186801
- [55] Matsugatani A and Watanabe H 2018 Connecting higher-order topological insulators to lower-dimensional topological insulators *Phys. Rev. B* **98** 205129
- [56] Franca S, van den Brink J and Fulga I C 2018 An anomalous higher-order topological insulator *Phys. Rev. B* **98** 201114(R)
- [57] You Y, Devakul T, Burnell F J and Neupert T 2018 Higher-order symmetry-protected topological states for interacting bosons and fermions *Phys. Rev. B* **98** 235102
- [58] Lin M and Hughes T L 2018 Topological quadrupolar semimetals *Phys. Rev. B* **98** 241103(R)
- [59] Călugăru D, Juričić V and Roy B 2019 Higher-order topological phases: A general principle of construction *Phys. Rev. B* **99** 041301(R)
- [60] Trifunovic L and Brouwer P W 2019 Higher-Order Bulk-Boundary Correspondence for Topological Crystalline Phases *Phys. Rev. X* **9** 011012
- [61] Liu F, Deng H Y and Wakabayashi K 2019 Helical Topological Edge States in a Quadrupole Phase *Phys. Rev. Lett.* **122** 086804
- [62] Yang Y B, Li K, Duan L M and Xu Y 2019 Type-II quadrupole topological insulators arXiv:1910.04151
- [63] Park M J, Kim Y, Cho G Y and Lee S 2019 Higher-Order Topological Insulator in Twisted Bilayer Graphene *Phys. Rev. Lett.* **123** 216803
- [64] Sheng X L, Chen C, Liu H, Chen Z, Yu Z M, Zhao Y X and Yang S A 2019 Two-Dimensional Second-Order Topological Insulator in Graphdiyne *Phys. Rev. Lett.* **123** 256402
- [65] Li H and Sun K 2020 Pfaffian Formalism for Higher-Order Topological Insulators *Phys. Rev. Lett.* **124** 036401
- [66] Huang B and Liu W V 2020 Floquet Higher-Order Topological Insulators with Anomalous Dynamical Polarization *Phys. Rev. Lett.* **124** 216601
- [67] Zeng Q B, Yang Y B and Xu Y 2020 Higher-order topological insulators and semimetals in generalized Aubry-André-Harper models *Phys. Rev. B* **101** 241104(R)
- [68] Lee C H, Imhof S, Berger C, Bayer F, Brehm J, Molenkamp L W, Kiessling T and Thomale R 2018 Topolectrical Circuits *Commun. Phys.* **1** 39
- [69] Luo K, Yu R and Weng H 2018 Topological Nodal States in Circuit Lattice *Research* **2018** 6793752
- [70] Lu Y H, Jia N Y, Su L, Owens C, Juzeliūnas G, Schuster D I and Simon J 2019 Probing the Berry curvature and Fermi arcs of a Weyl circuit *Phys. Rev. B* **99** 020302(R)
- [71] Yang Y B, Qin T, Deng D L, Duan L M and Xu Y 2019 Topological Amorphous Metals *Phys. Rev. Lett.* **123** 076401
- [72] Zeng Q B, Yang Y B and Xu Y 2020 Topological phases in non-Hermitian Aubry-André-Harper models *Phys. Rev. B* **101** 020201(R)
- [73] Jiang H, Lang L J, Yang C, Zhu S L and Chen S 2019 Interplay of non-Hermitian skin effects and Anderson localization in nonreciprocal quasiperiodic lattices *Phys. Rev. B* **100** 054301
- [74] Ningyuan J, Owens C, Sommer A, Schuster D and Simon J 2015 Time- and Site-Resolved Dynamics in a Topological Circuit *Phys. Rev. X* **5** 021031
- [75] Albert V V, Glazman L I and Jiang L 2015 Topological Properties of Linear Circuit Lattices *Phys. Rev. Lett.* **114** 173902
- [76] Luo K, Feng J, Zhao Y X and Yu R 2018 Nodal Manifolds Bounded by Exceptional Points on Non-Hermitian Honeycomb Lattices and Electrical-Circuit Realizations arXiv:1810.09231
- [77] Zhu W W, Long Y, Chen H and Ren J 2019 Quantum valley Hall effects and spin-valley locking in topological Kane-Mele circuit networks *Phys. Rev. B* **99** 115410
- [78] Zhang Z Q, Wu B L, Song J and Jiang H 2019 Topological Anderson insulator in electric circuits *Phys. Rev. B* **100** 184202
- [79] Haenel R, Branch T and Franz M 2019 Chern insulators for electromagnetic waves in electrical circuit networks *Phys. Rev. B* **99** 235110
- [80] Ezawa M 2019 Electric circuits for non-Hermitian Chern insulators *Phys. Rev. B* **100** 081401(R)
- [81] Hofmann T, Helbig T, Lee C H, Greiter M and Thomale R 2019 Chiral voltage propagation and calibration in a topolectrical Chern circuit *Phys. Rev. Lett.* **122** 247702
- [82] Liu S, Ma S, Yang C, Zhang L, Gao W, Xiang Y J, Cui T J and Zhang S 2020 Gain- and Loss-Induced Topological Insulating Phase in a Non-Hermitian Electrical Circuit *Phys. Rev. Applied* **13** 014047
- [83] Olekhno N A, Kretov E I, Stepanenko A A, Ivanova P A, Yaroshenko V V, Puhtina E M, Filonov D S, Cappello B, Matekovits L and Gorlach M A 2020 Topological edge states of interacting photon pairs emulated in a topolectrical circuit *Nat. Commun.* **11** 1436
- [84] Hirota R and Suzuki K 1970 Studies on lattice solitons by using electrical networks *Phys. Soc. Jpn.* **28** 1366
- [85] Hirota R and Suzuki K 1973 Theoretical and experimental studies of lattice solitons in nonlinear lumped networks *Proc IEEE* **61** 1483
- [86] Liu W M and Kengne E 2019 *Schrödinger Equations in Nonlinear Systems* (Singapore: Springer)
- [87] Qi X L, Hughes T L and Zhang S C 2008 Topological field theory of time-reversal invariant insulators *Phys. Rev. B* **78** 195424

- [88] Fu L, Kane C L and Mele E J 2007 Topological Insulators in Three Dimensions *Phys. Rev. Lett.* **98** 106803
- [89] Fu L and Kane C L 2007 Topological insulators with inversion symmetry *Phys. Rev. B* **76** 045302
- [90] Pitaevskii L and Stringari S 2016 *Bose-Einstein Condensation and Superfluidity* (Oxford: Oxford University Press)
- [91] Ablowitz M J 2011 *Nonlinear dispersive waves: asymptotic analysis and solitons* (Cambridge: Cambridge University Press)
- [92] Tonso M, Morren J, de Haan S W H and Ferreira J A 2005 Variable inductor for voltage control in distribution networks, in the *11th European Conference on Power Electronics and Applications (EPE 2005)*
- [93] Liu M X, Zhang H, Chen G D and Gong W 2012 Analysis and Design of A New Numerical Control Variable Inductance *Chinese Journal of Electron Devices* **35** 4